

# Self-pulsing effect in chaotic scattering

C. Jung<sup>1</sup>, C. Mejía-Monasterio<sup>1†</sup>, O. Merlo<sup>2</sup> and T. H. Seligman<sup>1</sup>

<sup>1</sup>Centro de Ciencias Físicas, Universidad Nacional Autónoma de México, Cuernavaca, Morelos, México

<sup>2</sup> Institut für Physik der Universität Basel, Basel Switzerland

E-mail: carlos.mejia@uninsubira.it

**Abstract.** We study the quantum and classical scattering of Hamiltonian systems whose chaotic saddle is described by binary or ternary horseshoes. We are interested in parameters of the system for which a stable island, associated with the inner fundamental periodic orbit of the system exists and is large, but chaos around this island is well developed. In this situation, in classical systems, decay from the interaction region is algebraic, while in quantum systems it is exponential due to tunneling. In both cases, the most surprising effect is a periodic response to an incoming wave packet. The period of this self-pulsing effect or scattering echoes coincides with the mean period, by which the scattering trajectories rotate around the stable orbit. This period of rotation is directly related to the development stage of the underlying horseshoe. Therefore the predicted echoes will provide experimental access to topological information. We numerically test these results in kicked one dimensional models and in open billiards.

Submitted to: *New J. Phys.*

PACS numbers: 05.45.Mt, 03.65.Nk

† Present address: Center for Nonlinear and Complex Systems, Università degli Studi dell'Insubria, Via Valleggio 11, 22100 Como, Italy

## 1. Introduction

The purpose of any scattering experiment is to learn something about the dynamics of the total system consisting of projectile and target in situations, where the direct observation of the dynamics of this total system is not possible or difficult. Then we need to evaluate the asymptotic scattering data to gain this desired insight. Thereby we are lead to the inverse scattering problem. Traditionally this expression is used for the reconstruction of the potential or of the Hamiltonian. For chaotic systems, however, the reconstruction of other quantities like for example characteristics of the chaotic saddle or chaotic invariant set might also be worth while and more realistic [1]. Even if possible, reconstructing the potential first and using it to reconstruct the dynamics and then investigating this reconstructed dynamics to get the information on the chaotic saddle includes a lot of sources for errors and ambiguities. Therefore it is attractive to develop strategies to extract the properties of the chaotic saddle directly from the scattering data. In this spirit the most complete information would be the reconstruction of the complete knowledge of all properties of the chaotic saddle of the system directly from asymptotic measurements. For system of two degrees of freedom (including time-dependent systems with one degree of freedom) this chaotic set might be represented by a horseshoe [2] construction of an iterated map, typically on a surface of section appropriately chosen. The inverse problem turns into the problem of reconstructing the properties of this horseshoe from the knowledge of scattering data.

First steps in this direction have been taken in [1] for kicked systems in one dimension as well as for systems with one open degree of freedom and one closed vibrational degree of freedom [3]. An independent alternative has been presented in [4]. All this work is based on the evaluation of the fractal structure of scattering functions where the hardest problem is the recognition of the hierarchical level of all intervals of continuity. Once we have done this step we can reconstruct the branching tree of the underlying fractal, measure all its scaling factors and apply the thermodynamical methods [5] to extract quantitative measures of chaos. For the measurement of these scattering functions the simultaneous preparation and measurement of canonically conjugate variables is necessary. Therefore all these methods are essentially classical and might at best work in the deep semi-classical domain of wave mechanics. In addition these methods are useful only for complete or near-complete horseshoes.

In contrast in the present paper we present a completely different idea which is based on the self-pulsing effect of chaotic scattering systems with horseshoes of a low development stage. The present method has the pleasant property that it does not require the simultaneous measurement of conjugate variables. Therefore it works similarly in classical and in quantum dynamics. The only important difference between the classical and the wave versions is, that due to tunneling in wave mechanics the interior of KAM islands is also explored, which is inaccessible to asymptotic observation in the classical case. For our argument it is essential that the system can be described by an iterated map on a two-dimensional domain. This implies the same restriction to

two dimensions, that we encountered in previous work [1, 3, 4].

Preliminary results along for the line of argument we shall present were given in a letter [6] for kicked systems. At present experiments are in progress in Darmstadt [7] applying our idea to the propagation of electromagnetic waves in an open superconducting cavity that can be viewed as an open two-dimensional billiard.

We shall present both kicked systems for their simplicity and scattering billiards because of the ongoing experiments and because of their relevance for mesoscopic structures. The surface of section will be a stroboscopic map in the first case and a Birkoff map in the second one. We shall concentrate on geometries that lead to low order horseshoes, in fact limiting our considerations to second and third order, though the basic idea is not subject to such a limitation. Furthermore we shall make extensive use of the parametrization of the development of a horseshoe as given in [8], and we shall only be concerned by degrees of development considerably smaller than one half, which insures, that a large stable island around the inner fixed point still exists. We shall show, that this island with its characteristic fractal surroundings rotate at a rate defined by the formal development parameter of the horseshoe. This gives rise to the suspicion, that this time of revolution can be measured by studying pulsed reverberance of the scattering system, which we name scattering echoes (to distinguish them from Loschmidt echoes). Numerical simulation shows, that it should be possible to measure such echoes.

In the next section we shall proceed to discuss the way such echoes may occur, and in the third section we derive the formulae for the relation between formal development parameters of the horseshoe and the period of the echoes. We then proceed to discuss examples leading to binary and ternary horseshoes. For kicked systems we discuss both the classical and wave-mechanical part, while we limit ourselves to a classical discussion of scattering billiards, as these present a fine example where reliable calculations are extremely expensive, and will not be able to replace the experiment in the microwave cavity. We will then draw some conclusions and give an outlook.

## 2. Scattering Echoes

In this section, we shall demonstrate the appearance of echoes in the scattering of any typical two degrees of freedom Hamiltonian scattering system described by a binary or ternary horseshoe with a low degree of development, *i. e.* with a large central stable island.

We first consider a scattering system whose chaotic saddle is described in some appropriate Poincaré map by a binary horseshoe, *i.e.* one having two fixed points. One of the fixed points is normal hyperbolic for any set of values of the physical parameters of the system. It couples the complicated dynamics inside the interaction region with the regular dynamics in the asymptotic region. For this reason, this unstable fixed point is usually called the *exterior fixed point*. Its invariant manifolds trace out the horseshoe, from whose topological structure at least an approximate symbolic dynamics can be

obtained [1, 8]. This forms the core of the method presented in this paper.

The intersections between the stable and unstable manifolds of the horseshoe form the so-called homoclinic tangle. The fractal and hierarchical arrangement of the homoclinic intersections are responsible for the chaotic motion inside the scattering region and surrounds the second fixed point of the Poincaré map, thus called the *inner fixed point*. Contrary to the exterior fixed point, the stability of the inner fixed point depends on the values of physical parameters of the system. For typical systems, the Poincaré map shows a complete KAM scenario: First the inner fixed point is stable, surrounded by KAM surfaces. Eventually, those KAM surfaces break into chains of secondary islands and chaotic layers which for higher levels of development fuse into one large homoclinic tangle. For some values of the parameters, the inner fixed point changes its stability through a period-doubling bifurcation.

For the method presented here the existence of an inner stable island is essential and therefore, we shall focus on a region in the parameter space for which the inner fixed point is stable and surrounded by a large primary island of stability with the generic region of secondary stable islands and chaos surrounding it. In Fig. 1 we show a schematic representation of the structure of the Poincaré map of a generic system in the situation just described. The exterior fixed point is represented by a cross and its unstable dynamics in its vicinity is indicated by the red arrows. The homoclinic tangle of the exterior fixed point surrounds the stable island. Beyond the last KAM surface of the primary island the non-trivial scattering trajectories traverse what we may call the *chaotic scattering layer*.

The scattering layer extends to infinity, covering the whole domain of the map outside of the last KAM surface. However, the part of the scattering layer of interest for the scattering process corresponds to the one whose energy domain in the asymptotic region coincides with the energy domain for which the singular structure in scattering functions appear. This chaotic scattering layer is actually the region of the homoclinic tangle represented in Fig. 1, as the gray ring around the stable island. The gray strips that extend to infinity correspond to region in which the incoming and outgoing trajectories enter or leave the chaotic scattering layer and are the region over which the infinity of tendrils of the stable and unstable manifolds of the outer fixed point are spread. The incoming trajectories not belonging to this gray layer will either bounce back to the asymptotic region immediately or travel around the stable island without entering into the chaotic scattering layer. Those trajectories will be scattered in what are usually called direct processes.

Let us describe the scattering process as viewed on the Poincaré surface of section sketched in Fig. 1. We focus on incoming scattering trajectories that start close to the stable manifold. When these trajectories enter the chaotic scattering layer they rotate around the stable island. This rotation is characterized by the winding number of the outermost KAM surface. Its effects are felt over the full scattering layer and as we shall show in the next section, it can be directly related to the topology of the underlying chaotic saddle.

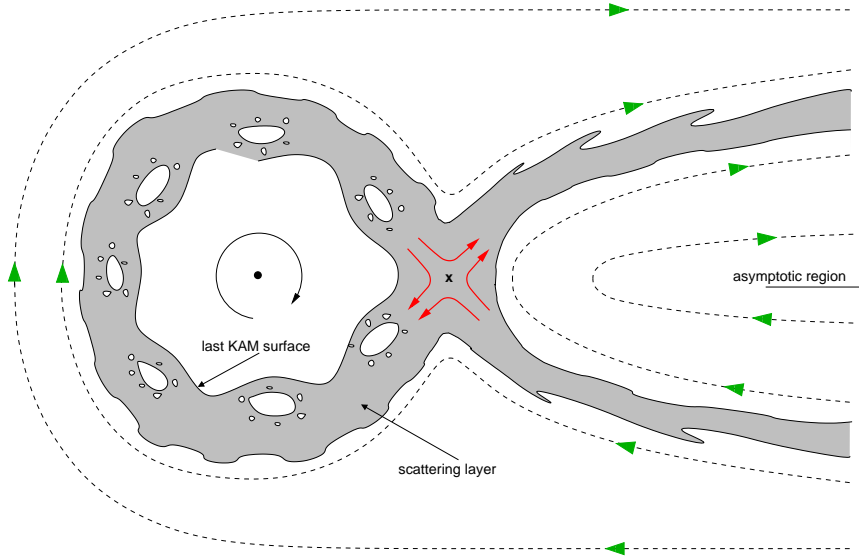


**Figure 1.** Schematic representation of the generic surface of section for a scattering system described by a binary horseshoe. The green arrow lines represent the flow of the trajectories over the surface of section.

As is well known [9], in their rotation around the island the trajectories always return to the vicinity of the exterior fixed point. Depending on the initial conditions, after one revolution some of the trajectories will leave the homoclinic tangle along the unstable manifold. The rest will continue in their rotation to complete a second revolution around the island. When the remaining trajectories return to the vicinity of the exterior fixed point, part of them will in turn exit the chaotic scattering layer to the asymptotic region. This process will continue *ad infinitum*.

The key observation is the following: Any trajectory starting close to the stable manifold will leave the chaotic scattering layer after an integer number of revolutions around the stable island. As a result, if we measure the asymptotic outgoing flux resulting from a narrow packet of incoming trajectories, we shall observe that the flux intensity oscillates in time. Clearly, the time between two successive maxima of the outgoing flux will correspond to the period of time a typical trajectory in the scattering layer needs to complete a rotation around the island or equivalently, to the return time to the neighbourhood of the exterior fixed point. The minimal return time corresponds to the trajectories close to the surface of the island which is most sticky and thereby, determines the time between the observed outgoing pulses, *i.e.* the scattering echoes. In a typical situation the return times of the trajectories in the chaotic scattering layer increase monotonously with the distance from the center of the stable island. Therefore, the time between successive echoes will be determined by the mean orbital period of rotation of the trajectories rotating close to the surface of the island. The width of the echoes in the outgoing flux will be related to the intrinsic dispersion of the packet of incoming trajectories in the chaotic scattering layer. Thus, the appearance of scattering

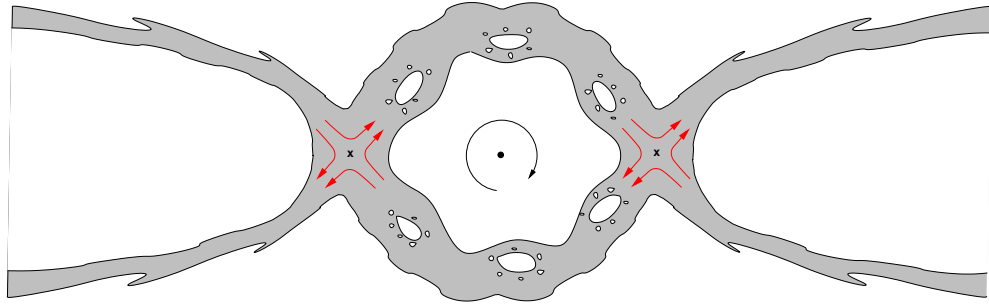


**Figure 2.** Schematic representation of the generic surface of section for a scattering system described by a ternary horseshoe.

echoes is typical for 2-dimensional Hamiltonian scattering systems, where the chaotic invariant set is represented by a horseshoe of low development stage.

Hamiltonian scattering systems in which the Poincaré map possesses 3 fixed points can be described by a ternary horseshoes. We concentrate on cases where there exist two exterior normal hyperbolic fixed points. This implies the existence of two fractal bundles of tendrils of stable manifolds along which trajectories can enter the chaotic layer and another two fractal consisting of unstable manifolds for the exit. We shall continue to call the tangle formed by the intersections of the invariant manifolds of the two exterior fixed points "homoclinic tangle", though it clearly contains both homoclinic and heteroclinic intersections. It surrounds the inner fixed point whose stability is determined by the physical parameters of the system. In Fig. 2 we show a schematic representation of the structure of the Poincaré map of a generic system described by a symmetric ternary horseshoe. In the region of parameter space where the inner fixed point gives rise to a well developed island of stability surrounded by a chaotic scattering layer, it is possible to follow the same line of argumentation as above. This leads to the conclusion that the existence of scattering echoes remains generic. The time between echoes is again given by the return time in the chaotic scattering layer to the given exterior fixed point. The main difference with the binary case is that for the symmetric ternary case there are two outgoing manifolds near to which the self-pulsing can be measured. If we perform such an experiment with a narrow packet of incoming trajectories from one side the scattering echoes shall appear in both outgoing manifolds in counter-phase.

On the quantum level we expect to see the same scattering echoes. Actually, we find that the echoes are more clean-cut in the quantum regime, and we shall see that this is due to tunneling. While forbidden for classical trajectories the quantum probability can penetrate KAM surfaces and settle on inner regions of the classical island. Therefore, if the quantum probability rotates around the island at a smaller distance from the center, the period of the quantum echoes will systematically differ from the classical one. The quantum probability will feel the winding number of inner KAM surfaces and send this information out through the scattering echoes. This phenomenon is interesting by itself. By measuring the period of the quantum echoes we are able to probe regions

in phase space that are inaccessible to classical scattering and obtain information about the topology of the classical chaotic saddle by controlling the limit  $\hbar \rightarrow 0$ .

### 3. The period of scattering echoes

The central point of the method developed in this paper is the connection between the period of the scattering echoes and the development stage of the horseshoe. As has been discussed in the previous section, this time corresponds to the inverse of the mean winding number or orbital period in the chaotic scattering layer. Thus the period of the scattering echoes is given in units of the mean return time to the surface of section. To unravel its connection with the topology of the underlying chaotic invariant set we shall use the formal development parameter  $\alpha$  as a measure of the development of the horseshoe. It measures the penetration depth of the tendrils into the interior of the fundamental area of the horseshoe and therefore contains the information on the primary homoclinic intersections. This tells us the universal aspects of the topology of the hyperbolic component of the horseshoe. The parameter takes values from 0 corresponding to a separatrix loop, to 1 when the horseshoe becomes complete. For a detailed definition of the development parameter and a discussion of the development stages of incomplete horseshoes as well as for the terminology we use, we refer the reader to Refs. [1, 8].

The relation of the development parameter  $\alpha$  to the winding number in the chaotic scattering layer is most easily established if  $\alpha = 1/k^n$ , where  $k$  is the order of the horseshoe. Thus, without loss of generality, we shall stick to this case and then invoke continuity arguments to close the gaps.

Before continuing with the description of the method, there are some properties of the horseshoe construction, illustrated in Fig. 3, we would like to point out:

- (i) The horseshoe construction is created by the intricate intersections between the stable and unstable manifolds of the exterior fixed points. The horseshoe exists in a surface of section and its outer unstable part forms the chaotic scattering layer. The invariant manifolds of the exterior fixed points never enter any KAM island.
- (ii) Any point on the unstable invariant manifold converges to the exterior fixed point as time  $t \rightarrow -\infty$ . Any point on the stable invariant manifold converges to the exterior fixed point as time  $t \rightarrow \infty$ .
- (iii) The labeling of the different tendrils of the horseshoe is quite convenient as due to the invariance of the manifolds, each tendril is the image and the pre-image of other tendrils under the Poincaré map. For the unstable manifold tendril  $n$  is the image of  $n - 1$ . For the stable manifold tendril  $n$  is the image of  $n + 1$ .

In what follows we shall stick to the binary horseshoe case and briefly discuss at the end the modifications of the method for the ternary case. By definition, if for a binary horseshoe  $\alpha = 2^{-n}$ , the first tendril of one of the invariant manifolds is intersected by the tip of the  $n$ -th tendril of the other one in two points only. We label the different tendrils

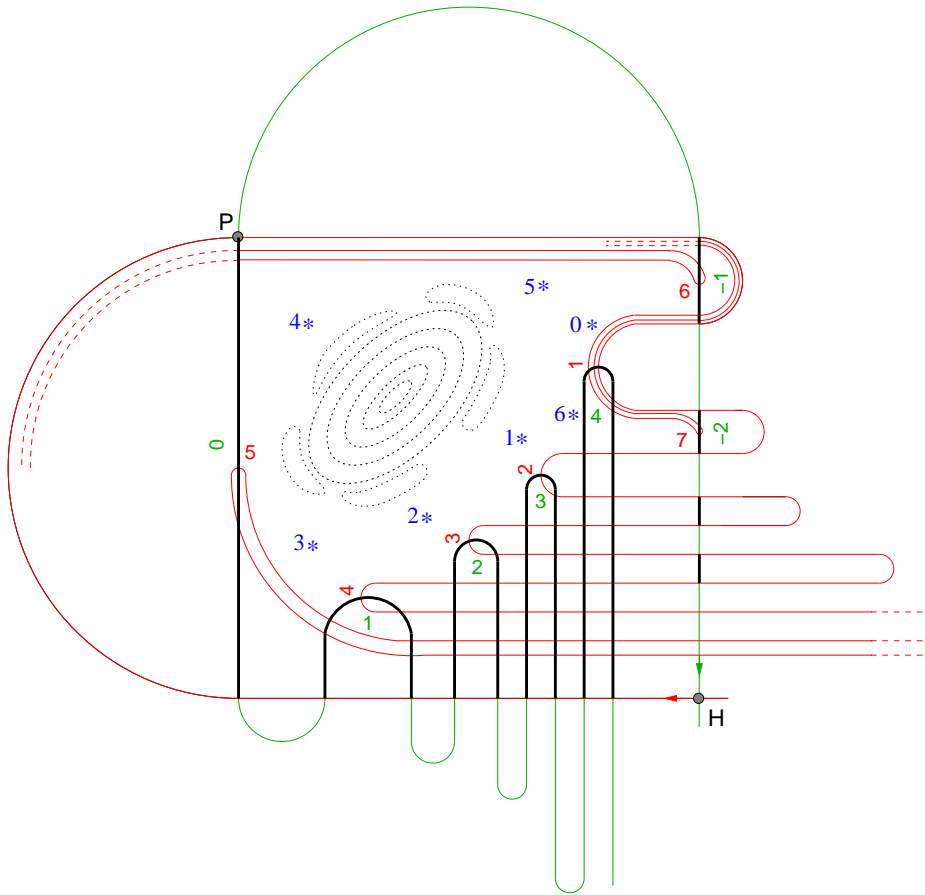


**Figure 3.** Topology of a horseshoe for  $\alpha = 1/16$ . The point  $H$  is the exterior fixed point. Its invariant manifolds the unstable in red and stable in green, first intersect in the primary intersection point  $P$ . The successive tendrils are labeled starting from  $P$ . The tendrils of the stable manifold have been emphasized in black.

starting from the so-called primary intersection indicated by the letter  $P$  in Fig. 3. There we show schematically the topology corresponding to an incomplete horseshoe with  $\alpha = 2^{-4}$ . Thus, tendril 1 of the unstable invariant manifold (shown in red) is intersected by the tip of the 4-th tendril of the stable manifold (in green) in two points.

In Fig. 3, we have emphasized the tendrils of the stable manifold in black. From property (iii) the tendril 1 of the stable manifold is the image of tendril 2 and pre-image of tendril 0. Tendril 2 is in turn the image of tendril 3 while tendril 0 is the pre-image of tendril  $-1$  and so on back and forward *ad infinitum*. Due to this hierarchy, an intersection between tendril  $n$  of the unstable manifold and tendril  $m$  of the stable manifold labeled by  $(n:m)$  is the image of the intersection  $(n-1:m+1)$  and pre-image of  $(n+1:m-1)$ .

We now have all the information we need to relate the development of the horseshoe in terms of the parameter  $\alpha$  to the orbital period. By construction, tendril 1 of any of the invariant manifolds is in between tendrils  $-1$  and  $-2$  of the other manifold. If a generic trajectory is started in the vicinity of the unstable tendril 1 (represented by



the sequence of stars in Fig. 3), after one iteration of the Poincaré map it will be in the vicinity of the unstable tendril 2. After a second iteration, the trajectory will be near the unstable tendril 3 and so on. *A priori*, we do not know which of the unstable tendrils will be again in the vicinity of the unstable tendril 1, but we do know that this trajectory will have almost completed a revolution around the inner stable island when it reaches the vicinity of the stable tendril  $-1$ , and a little bit more than one revolution when it reaches the vicinity of the stable tendril  $-2$ . A development  $\alpha = 2^{-n}$  implies an intersection  $(1 : n)$ . Since the stable tendril  $-1$  is the  $(n+1)$ -th image of the stable tendril  $n$ , the unstable tendril which intersects the stable tendril  $-1$  is the  $(n+2)$ -th. Thus, if the trajectory was started in the vicinity of the unstable tendril 1, and since the unstable tendril  $n+2$  is the  $(n+1)$ -th image of 1, this trajectory will have almost completed a revolution in  $n+1$  iterations of the Poincaré map. Equivalently, this trajectory will have completed a little bit more than one revolution after  $n+2$  iterations of the Poincaré map.

Concerning our interest in the average behaviour of the trajectories close to the surface of the island, we have obtained the following: If the development of the underlying horseshoe is  $\alpha = 2^{-n}$ , the orbital period of the scattering trajectories is approximately  $n+3/2$  and we cast this result into the form

$$T = -\log_2 \alpha + \frac{3}{2} . \quad (1)$$

The mean period  $T$  in eq. 1 is given in units of the return time to the surface of section  $\tau_{SOS}$  which corresponds to the time spend in one iteration of the Poincaré map. For time periodic systems, the Poincaré map is the stroboscopic map and thus, the return time to the surface of the section is constant. For systems which are not periodic in time, the units of  $T$  can be taken as the mean return time to the surface of section in the chaotic scattering layer. The development of the horseshoe, related to the dynamics of the system, does not depend on the surface of section we select. This is tantamount to the fact that the mean  $\tau_{SOS}$  does not depend on the surface we choose.

In the derivation of eq. 1 we have not used any particular model. Therefore, this relation between the mean orbital period and the topology of the hyperbolic component of the horseshoe given in terms of the development parameter  $\alpha$  is universal for Hamiltonian scattering systems described by a binary horseshoe. Inverting eq. 1 we obtain

$$\alpha(T) = 2^{(\frac{3}{2}-T)} . \quad (2)$$

However, since  $\alpha$  is given in terms of the revolutions of the scattering trajectories around the stable island, the application of eqs. 1 and 2 is limited to the situation where a central stable island actually exist. This condition is formally fulfilled for  $\alpha < 1/2$  [8], but practically this method is probably limited to cases in which the horseshoe is in a stage of low development say with  $\alpha \approx 1/4$  or smaller.

For the case of Hamiltonian scattering systems described by a symmetric ternary horseshoe, following the same arguments as for the binary case, the formal development

parameter (called  $\beta$  to distinguish it from the binary case) is related with the orbital period by

$$\beta(T) = 3^{(\frac{3}{2}-T)/2} . \quad (3)$$

In eq. 3, the base 3 comes from the fact that the horseshoe is ternary and the  $1/2$  in the exponent is due to the existence of two exterior fixed points.

#### 4. Examples

In this section we shall consider both binary and symmetric ternary situations in detail using kicked one-dimensional systems and open two-dimensional billiards as examples. On one hand we shall concentrate on a billiard that gives rise to a binary horseshoe, while another one corresponding to a ternary horseshoe will be presented in the context of a superconducting experimental realization performed presently at Darmstadt [7]. On the other hand we shall study in detail a kicked system that gives rise to a ternary horseshoe giving considerably more detail than in the short discussion of the binary horseshoe in Ref. [6]. For kicked systems classical and quantum dynamics are easily solved numerically. For billiards the classical analysis is simple, while the numerical analysis of the wave equation in scattering situations is more delicate, and little previous work has been done. Here we shall limit our analysis of such systems to the classical case and leave the study of wave mechanics to the experimental analysis.

##### 4.1. Binary horseshoe

In this section we shall study the classical echoes that appear in the scattering of a classical open elastic billiard. For this we could think of using the well known three discs problem [16], but this system has serious disadvantages; the principal one is that the low development degree of the horseshoe, that we desire cannot be reached. While the shadowing of orbits from one disc to the next will lead to incomplete horseshoe scenarios due to pruning, stable islands do not develop. This can be intuitively understood from the fact that even when the circles osculate such islands are absent [17], and a numerical analysis confirms that the horseshoes we need are not obtainable. We therefore look for a bottle shaped billiard with a single opening. Its boundary consist in an arc of ellipse to the left (bottom of the bottle) and a quartic polynomial curve properly connected (for the neck of the bottle). For practical purposes we use only half the bottle split along its length. Therefore, at the lower part the billiard will consist in the line  $y(x) = 0$ . The exact form of the upper boundary is

$$y(x) = \Delta \begin{cases} (1 - x^2/\beta^2)^{1/2} & , \quad x < 0 \\ (\frac{x^4}{16\beta^4(1-\gamma)} - \frac{x^2}{2\beta^2} + 1) & , \quad x \geq 0 \end{cases} . \quad (4)$$

The shape of the bottle is shown inside Fig. 4 where the length parameters  $\beta$ ,  $\gamma$  and  $\Delta$  are indicated. The parameters  $\Delta$  and  $\beta$  correspond to the semi-axes of the ellipse;

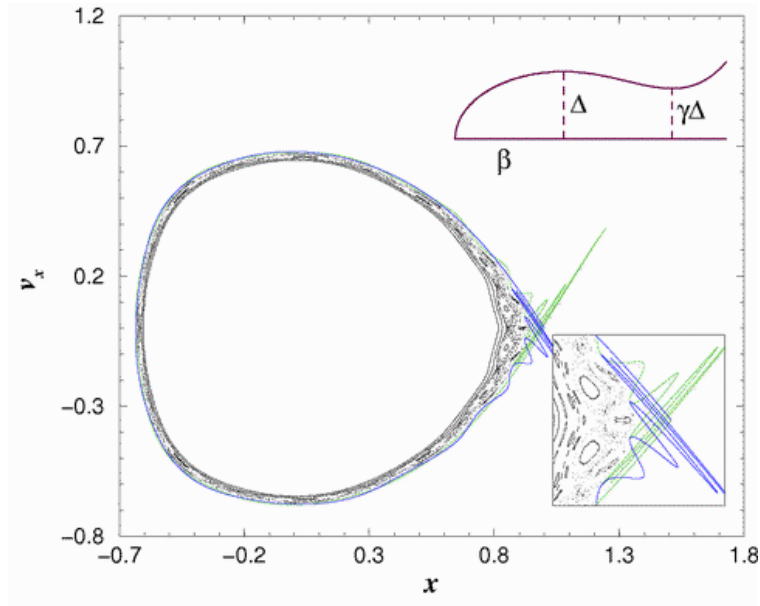


**Figure 4.** Classical phase portrait for the bottle billiard for  $\Delta = 0.35$ ,  $\beta = 1$  and  $\gamma = 0.75$ . The horseshoe with development  $-\log_2 \alpha = 11$  is shown in blue (stable manifold) and green (unstable manifold). The shape of the billiard is shown at the top right of the figure where the dashed lines corresponds to the stable (interior) and unstable (exterior) periodic orbits. In the inset we show an amplification of the region around the exterior fixed point.

$\gamma \in [0, 1)$  corresponds to the size of the opening in units of  $\Delta$ . This boundary is a  $\mathcal{C}^2$  function everywhere in its domain.

The bottle has two fundamental periodic orbits corresponding to trajectories, which are normal to both the upper and lower boundaries. These orbits are shown as dashed lines in Fig. 4. The stability of the inner periodic orbit at  $x = 0$  depends on the local curvature of the boundaries and therefore, on the values of all the parameters. The exterior periodic orbit at  $x_n = 2\beta\sqrt{1 - \gamma}$  is unstable for any set of parameters. It couples the relevant part of the complicate dynamics in the interior of the bottle with the regular dynamics in the asymptotic region. In our surface of section the exterior periodic orbit will give a hyperbolic fixed point at  $(x, v_x) = (x_n, 0)$ . Its stable and unstable invariant manifolds constitute the horseshoe that for this billiard is binary. Therefore, by tuning the different parameters we can study the scattering process for different stages of development of the horseshoe. In Fig. 4 a Poincaré section for  $\Delta = 0.35$ ,  $\beta = 1$  and  $\gamma = 0.75$  is plotted. It shows a large stable island surrounded by a well developed scattering layer over which the corresponding horseshoe (in blue and green) is also shown. Each point in the surface of section correspond to the position  $x$  and  $x$ -component of the velocity  $v_x$  of a particle trajectory when it hits the lower ( $y = 0$ ) boundary of the billiard. For this case, the development of the horseshoe is  $-\log_2 \alpha = 11$ .

To study classical scattering in this model system, we have numerically solved the classical ray dynamics of scattering trajectories inside the billiard. To observe the

scattering echoes we have followed the *gedanken* experiment proposed in Sec. 2: We have prepared a narrow packet of initial conditions in phase space. Initially, the narrow packet is placed in the asymptotic region. Any trajectory initially not close to the incoming stable manifold of the horseshoe will either not enter the chaotic scattering layer or will enter but leave immediately in an uninteresting direct process. Since we are interested in those trajectories that enter the scattering layer the initial velocities  $v_x$  were chosen randomly in a small window around some appropriate value, such that the initial packet shadows the incoming stable manifold of the horseshoe. As ray dynamics trivially scales with energy, we fix the speed of all trajectories to one. Therefore,  $v_x$  can be interpreted as  $\cos \phi$  where  $\phi$  is the angle between the direction of the trajectory and the normal to the boundary in the position of collision. In Fig. 5-*a*, we show the classical density  $\rho_{\text{cl}}(x, t)$  as a function of position and time for  $\Delta = 0.35$ ,  $\beta = 1$  and  $\gamma = 0.75$ . Following the scattering process we can observe the initial narrow packet approaching the scattering region from the right. When the packet reaches the bottle neck at  $x_n = 1$  some trajectories are bounced back while the rest enter the bottle. On the surface of section, these trajectories rotate in the scattering layer, around the stable island. This rotation is clearly seen as an oscillation in the  $x$ - $t$  plane. After one oscillation (corresponding to one revolution around the stable island) some of the trajectories exit the scattering layer along the unstable manifold. The rest are bounced back at the neck staying in the scattering layer one more oscillation. After a second oscillation is completed the process is repeated *ad infinitum*. The appearance of periodic pulses, *i. e.* scattering echoes in the decay of the number of trajectories remaining inside the bottle is evident.

The period of these echoes can be easily extracted by measuring the intensity of scattered trajectories as they cross some position in the asymptotic region. In Fig. 5-*b* we plot the normalized outgoing flux of scattered trajectories as a function of time  $P(t)$  measured at  $x = 20$ . The scattering echoes are clearly visible and we obtain a value for their period of  $\tau = 7.9 \pm 0.7$ . The decay underlying the oscillations in  $P(t)$  is of power-law nature, with a power of  $\approx 2$  which is well within the expected limits [18]. It is worthwhile mentioning, that we do not claim that this power law is asymptotic, but it seems well defined for almost two decades. We detect at least twenty oscillations, that represent echoes, so these correspond to a significant transient. Diffusion in the chaotic layer spreads the remaining packet and thus damps the echoes.

As discussed in the previous section, before comparing  $\tau$  with the value predicted by eq. 1, we must divide  $\tau$  by the mean return time to the surface of section  $\tau_{SOS}$ . Measuring the return time to the surface of section of the trajectories rotating around the stable island we have numerically obtained  $\tau_{SOS} = 0.635$  and then,  $\tau/\tau_{SOS} = 12.44 \pm 1.1$  which is in excellent agreement with theoretical prediction of  $T = 12.5$ . However, there does not exist a direct procedure by which  $\tau_{SOS}$  can be experimentally obtained from asymptotic data. Therefore, it would be desirable to test our method using exclusively quantities that can be measured or calculated from asymptotic experimental data. Unfortunately this seems to be quite difficult. Using techniques developed in [4] we can

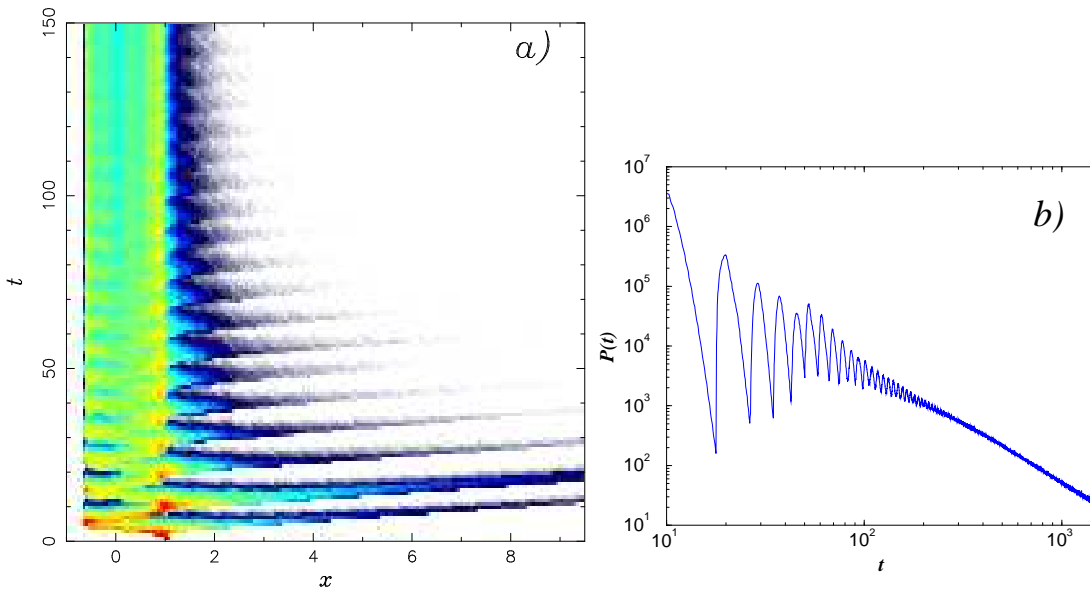


**Figure 5.** *a)* Classical density distribution in space and time  $\rho_{\text{cl}}(x, t)$  for the bottle billiard in a logarithmic colour scale for the same parameters as in Fig. 4. The colour ramp increases from blue to red. White indicates very low densities. *b)* Outgoing flux of classical trajectories as a function of time  $P(t)$  measured at  $x = 20$ .

determine the period of the outer unstable orbit easily, but that is to crude an estimate. We shall have to use some physical understanding of the system, to get a typical time for interior evolution. In the case of a billiard, this would be the transversal size of the scattering region, and we may take  $\tau_{\text{SOS}} \approx 2\Delta$ , where  $\Delta$  is the biggest width of the bottle. In this way we obtain a period of  $\tau = 11.3 \pm 1.0$  which is still in agreement with the theoretical expectation if one recalls that  $T$  is also a mean value with an associated error of  $\pm 0.5$ . If the billiards walls are thin this number could be extracted from a scattering measurement, but obviously we have no guarantee, that this is true. So we have to have some physical insight at this point, which depends very much on the system. On the other hand the prediction, that scattering echoes are associated with low developed horseshoe does not depend on this point. We shall see later, that in situations where wave mechanics apply we may be able to overcome this problem.

To further test the method of Sec. 3, we have measured the period of the classical echoes for different sets of the billiard's parameters giving rise to horseshoes at different stages of development. Fixing the values of  $\beta = 1$  and  $\gamma = 0.85$  and varying the length of the stable periodic orbit  $\Delta$ , we have obtained horseshoes in stages of development from  $\alpha = 2^{-4}$  to  $\alpha = 2^{-14}$ . For each case we have measured the normalized outgoing flux  $P(t)$  and from it obtained a value for the period  $\tau$  of the scattering echoes. In table 1 we summarize the different realizations of the billiard. We do so, by comparing  $\tau$  in units of both, the period of the stable periodic orbit  $2\Delta$  and the mean return time to the surface of section  $\tau_{\text{SOS}}$ . In Fig. 6  $\tau$  is compared with the theoretical expectations of eq. 1. We want to remark that even when in all cases we find good agreement with

$\Delta$	$T(\alpha)$	$\tau/2\Delta$	$\tau/\tau_{SOS}$	$\tau_{SOS}$
0.6300	5.5	$5.5 \pm 0.6$	$5.5 \pm 0.6$	1.246
0.5925	6.5	$6.4 \pm 0.6$	$6.7 \pm 0.6$	1.135
0.5100	7.5	$7.2 \pm 0.8$	$7.3 \pm 0.8$	0.999
0.4730	8.5	$8.8 \pm 0.6$	$9.1 \pm 0.7$	0.920
0.4550	9.5	$8.7 \pm 1.0$	$9.1 \pm 1.0$	0.862
0.4100	10.5	$9.8 \pm 0.9$	$10.1 \pm 0.9$	0.791
0.3810	11.5	$10.7 \pm 1.3$	$11.2 \pm 1.4$	0.730
0.3665	12.5	$11.6 \pm 1.0$	$12.2 \pm 1.0$	0.697
0.3577	13.5	$12.8 \pm 1.1$	$13.5 \pm 1.1$	0.677
0.3250	14.5	$13.4 \pm 1.4$	$14.1 \pm 1.4$	0.618
0.3082	15.5	$14.9 \pm 1.5$	$15.7 \pm 1.5$	0.587
0.2800	19.5	$18.2 \pm 0.9$	$19.3 \pm 0.9$	0.529

**Table 1.** Comparison between the values obtained for the period  $\tau$  of the scattering echoes for the bottle billiard eq. 4 and those predicted by eq. 1  $T(\alpha)$ . We report  $\tau$  in units of the period of the stable periodic orbit (given by  $2\Delta$ ) and in units of the mean return time to the surface of section  $\tau_{SOS}$ . We report the parameter  $\Delta$  for which the horseshoes in different stages of development ( $-\log_2 \alpha$  from 4 to 14 and 18) are obtained. The obtained values for  $\tau_{SOS}$  are shown in last column. In all cases the other parameters were fixed to  $\beta = 1$  and  $\gamma = 0.85$ .

eq. 1 even better agreement is always found when the mean  $\tau_{SOS}$  is used.

For the case of scattering systems giving rise to a ternary horseshoe, we shall turn our attention in the next section mainly to kicked one-dimensional models described by the generic Hamiltonian of eq. 6. In a previous letter Ref. [6] we presented a short discussion of the appearance of classical and quantum scattering echoes in a kicked one-dimensional system that gives rise to a binary horseshoe. The system in question is described by potential profile given by

$$V(q) = \begin{cases} \frac{q^2}{2} + 1 & , \quad q < 0 \\ e^{-q}(q^2 + q + 1) & , \quad q \geq 0 \end{cases} . \quad (5)$$

For the detailed properties of the dynamics of this model we refer the reader to [6]. The technical details of the numerical computations will be discussed in the next section, in the context of a detailed treatment of ternary horseshoes. In order to gain more insight in the origin of the scattering echoes and more importantly, on the essential differences between the classical and quantum echoes, we have followed the evolution of the density distribution function in phase space  $\rho_{cl}(q, p)$  for the model system of eq. 5. Here,  $q$  and  $p$  are the canonically conjugated position and momentum variables.

We have created two animated movies, one for the classical density and other for an analogous quantum density in terms of the Husimi function [20]. We first turn our attention to the classical case. In movie 1, we show the time evolution of the

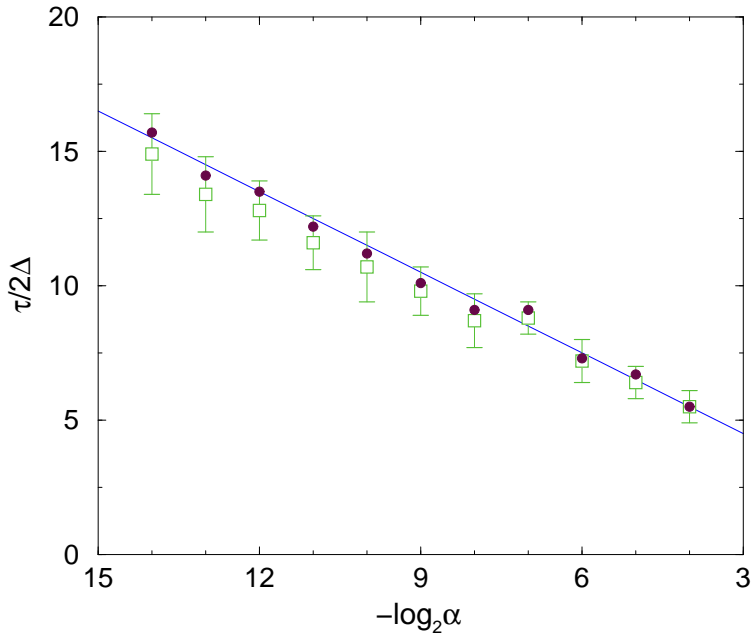


**Figure 6.** Period of the classical echoes  $\tau$  for the bottle billiard for the parameters listed in Tab. 1. We show both  $\tau/2\Delta$  (open squares) and  $\tau/\tau_{SOS}$  (solid circles). The straight line corresponds to the theoretical expectation  $T(\alpha)$  given in eq. 1.

classical density distribution initially consisting on a narrow packet of trajectories as a stroboscopic map on phase space. This distribution is presented in a quadratic colour-scale from blue to red. For each frame, the colour-code is rescaled so that it is possible to follow the evolution of the ever smaller density that is left inside the scattering region. Superposed in a gray-scale, the corresponding static phase portrait with the fractal layer of islands and KAM tori is shown. The value of  $A = 0.967$  (*c.f.* eq 6), used in this simulation was chosen because somewhere between this value and  $A = 1$ , the outermost KAM surface that appears close to the outermost dark structure surrounding the inner fixed point disintegrates.

The *movie* starts at the time when the packet reaches the interaction region along the incoming stable manifold. In a first passage, part of the packet bounces on the outside of the hyperbolic fixed point at  $(q, p) = (1, 0)$ . The rest enters the potential well where the packet moves around the inner fixed point at  $(q, p) = (0, 0)$ . After one rotation is completed, most of the packet leaves the scattering layer along the outgoing unstable manifold. A small part stays in the region of the homoclinic tangle and continues rotating around the island. We then see the density concentrated in a narrow region and slowly diffusing into the fractal zone of islands around the outermost KAM surface. This very diffusion also kills the echoes relatively rapidly because it widens the trapped part of the initial packet systematically. It is also responsible for the power-law decay, that is characteristic of such systems. A careful observation shows that each time the packet reaches the region around the unstable fixed point, part of the density is scattered

out forming an echo while the rest continues rotating with the scattering layer.

The process of emission of the echoes appears more clearly in the evolution of the quantum density. Under conditions similar to the classical case, we show in movie 2, the time evolution of the Husimi distribution of a Gaussian wave packet for  $A = 0.967$ ,  $\hbar = 0.01$  and  $\sigma = 2.5$ , initially at  $q_0 = 100$  and  $p_0 = -1.48$  (*c.f.* eq. 12). The Husimi distribution is presented in a quadratic colour-scale from blue to red, and again the colour-code is rescaled for each frame.

The direct part of the scattering of the distribution evolves quite similar to the classical case, bouncing off or going once around the island. The trapped part on the other hand shows a quite different behaviour. It penetrates the fractal area rapidly, so we can conclude, that tunneling rather than diffusion is the dominant mechanism, and indeed this process quickly extends inside the classically forbidden region of the central stable island. As we shall corroborate in next section, in the quantum case the echoes detect the winding numbers inside the outermost KAM-surface instead of those that characterize the scattering layer. For our examples and indeed in typical situations these are larger than on the outside, and therefore we can expect to see shorter periods as we have the opportunity to look *inside* the island. However, by decreasing the value of  $\hbar$ , the period of the quantum echoes will approach the estimate of eq. 1 leading to the possibility of a quantitative estimate of the development of the classical horseshoe. In movie 2 we clearly see how part of the quantum probability density is emitted in echoes. We also see that the formerly narrow packet that tunnels inside the island spreads in time over the invariant surface where it is trapped. This has the effect of gradually increasing the width of the echoes, though they persist much longer, than in the classical case. Again the observation of the scattering echoes will be possible only in an intermediate, though possibly quite long, time scale.

#### 4.2. Ternary horseshoe

We now turn our attention to ternary horseshoes. We shall concentrate on a second type of models that is on kicked one-dimensional scattering systems. The advantage of such models consists mainly in the fact that the dynamics is easily solved both in classical and in wave mechanics.

The model we study is described by a time dependent Hamiltonian given by

$$H(q, p, t) = \frac{p^2}{2} + A V(q) \sum_{n=-\infty}^{\infty} \delta(t - n) . \quad (6)$$

The time dependence consists of an infinite periodic train of delta pulses kicking with period 1 the otherwise free particle's trajectory. The physical parameter  $A$  determines the strength of the kick. Such periodically driven one-dimensional systems are formally equivalent to time-independent Hamiltonian systems with two degrees of freedom [10]. We thus expect to test the more general situation with reduced effort.

As Poincaré map for the classical problem we choose the stroboscopic map at times



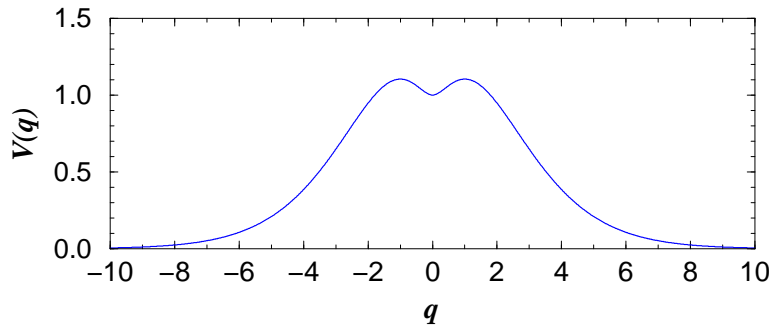


**Figure 7.** Potential profile of eq. 8.

$$t = n + 1/2$$

$$\begin{aligned} p_{n+1} &= p_n - AV'(q_n + p_n/2) \\ q_{n+1} &= q_n + p_n - AV'(q_n + p_n/2)/2. \end{aligned} \quad (7)$$

where  $V'$  stands for the derivative of the potential term. It gives the evolution of a classical trajectory from time  $n - 1/2$  to time  $n + 1/2$  and is symmetric with respect to time inversion.

The model in question is determined by a potential profile given by

$$V(q) = e^{-|q|}(q^2 + |q| + 1) \quad (8)$$

It consists of a finite potential well centered at  $q = 0$  enclosed by two potential barriers at  $q = \pm 1$ . At infinity, the potential decays exponentially to zero. This potential is shown in Fig. 7. The system has three fundamental periodic orbits and therefore, gives rise to a ternary horseshoe. Again, the stability of the interior periodic orbit at  $q = 0$  depends on the strength of the potential  $A$ . The exterior periodic orbits corresponding to the potential barriers, are unstable for any value of the physical parameter. In a phase portrait they appear as hyperbolic fixed points at  $(q, p) = (\pm 1, 0)$ . The ternary horseshoe is traced by the stable and unstable manifolds of both hyperbolic points.

We have extensively analysed the scattering process of this system for several values of the physical parameter  $A$  and thus, for horseshoes in different stages of development. In Fig. 8, we show the phase portrait and the underlying ternary horseshoe for four different values of  $A$ . We can observe how the horseshoe development decreases from  $\beta = 3^{-3}$  to  $\beta = 3^{-9}$  with the value of  $A$ . This occurs together with an enlargement of the stable island. The more developed the horseshoe is the more extended the scattering layer. These cases fulfill the conditions under which the appearance of echoes is expected, *i.e.*, in all cases of Fig. 8, there exist a large stable central island surrounded by a well developed chaotic scattering layer. Note also the decrease of the winding number with  $A$  in terms of the large chain of secondary islands living at the interior of the island. The stable island disappears at  $A = 4$  as it becomes unstable. Then the horseshoe is close to a development of  $\beta = 1/3$  and reaches complete development and thus hyperbolicity near  $A = 14.3225$ .

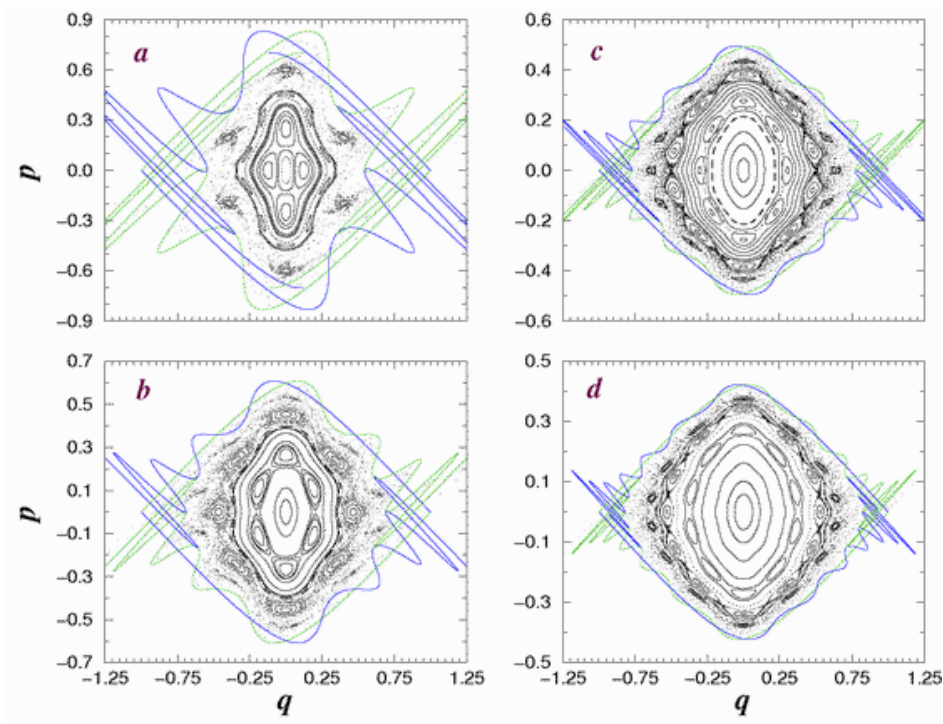


**Figure 8.** Horseshoe and phase portrait for the model system eq. 8, for several values of the formal development parameter  $-\log_3 \beta$ : a) 3 for  $A = 2.6$ , b) 5 for  $A = 1.54$ , c) 7 for  $A = 1.065$  and d) 9 for  $A = 0.8$ .

Before discussing the determination of the period of the scattering echoes we have numerically computed the mean orbital period  $T$  as a function of the physical parameter  $A$ . To this end, we have considered trajectories targeting the potential well from outside. This is important as we want to probe exclusively winding numbers of the scattering layer. We recall that by inverting eq. 3, we obtain an expectation value for the mean orbital period of the scattering trajectories rotating in the chaotic scattering layer close to the surface of the island. As a function of the formal development parameter  $\beta$ , the orbital period

$$T = -2 \log_3 \beta + \frac{3}{2}, \quad \beta = 3^{-n} \quad (9)$$

is, as before, given in units of  $\tau_{SOS}$ . Plugging in the values calculated for  $T(A)$  into eq. 9 we obtain the development parameter  $\beta$  as a function of the physical parameter  $A$ . In Fig. 9 we plot  $\beta(A)$  as a dashed line. The behaviour of  $\beta(A)$  coincides with the observations of Fig. 8 in which the horseshoe develops with  $A$ . Furthermore, we have directly determined the development of the horseshoe for several values of  $A$ . These values are shown as the squares in Fig. 9. The agreement with the behaviour of  $\beta(A)$  determined from the orbital period supports the identification of the period of the echoes with the mean orbital period.

Note that this result can be rather simply generalized, for the case of an asymmetric

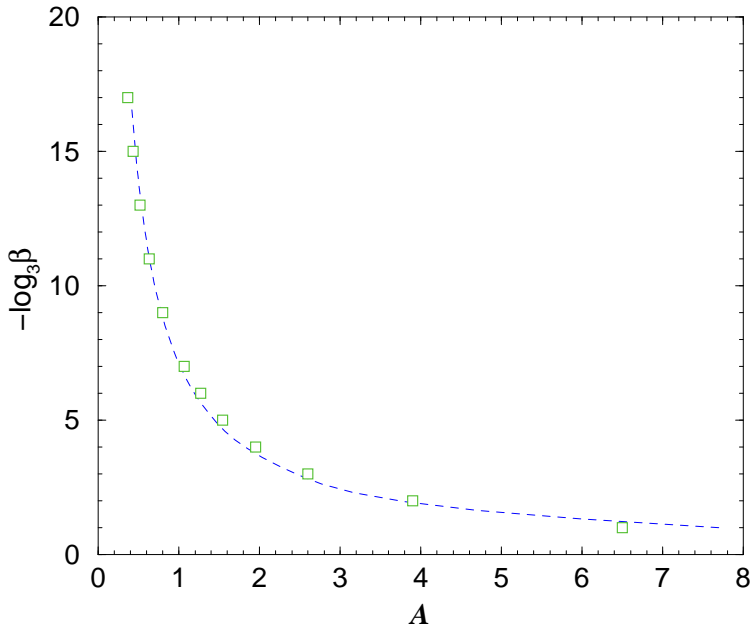


**Figure 9.** Development of the horseshoe  $-\log_3(\beta)$  as a function of the strength of the potential  $A$  for the potential of eq. 8. For the considered values of  $A$ , the squares correspond to the development  $\beta$  of the obtained horseshoe. The line corresponds to  $\beta(A)$  obtained from eq. 9, from the numerically determined mean orbital period  $T(A)$ .

ternary horseshoe with two outer fixed points yielding

$$T = -\log_3 \beta_1 - \log_3 \beta_2 + \frac{3}{2}. \quad (10)$$

To invert this equation we will need the relative phase of the echoes at both openings of the billiard; this can be achieved experimentally for open billiards, while it might be more difficult in other systems.

We shall now look at simulations to study the scattering echoes of the proposed symmetric ternary horseshoe. The situation is quite similar to the one discussed above for a binary horseshoe, except that the two external fixed points imply that the trajectories rotating around the stable island can now leave the scattering layer to both sides. Again we have prepared a narrow packet of initial conditions in phase space placed at the asymptotic region. Solving the dynamics through eq. 7 we follow the evolution of the classical density distribution  $\rho_{\text{cl}}(q, t)$  in the  $q$ - $t$  plane. In Fig. 10-*a*, we show  $\rho_{\text{cl}}(q, t)$  for  $A = 0.366$ . The packet was initially centered at  $(q, p) = (20, 0.9)$ , deep in the asymptotic region.

As in the binary case, the part of the classical density that enters the potential well oscillates inside and decays in echoes. The description of the scattering process is exactly the same as in the case of the binary horseshoe except that now the echoes are emitted with a period of  $T/2$  to one side and the other. As a consequence of the way we target the potential, if we measure the outgoing flux of trajectories  $P(t)$  at symmetric positions then we shall observe the echoes in counter phase. This can be observed

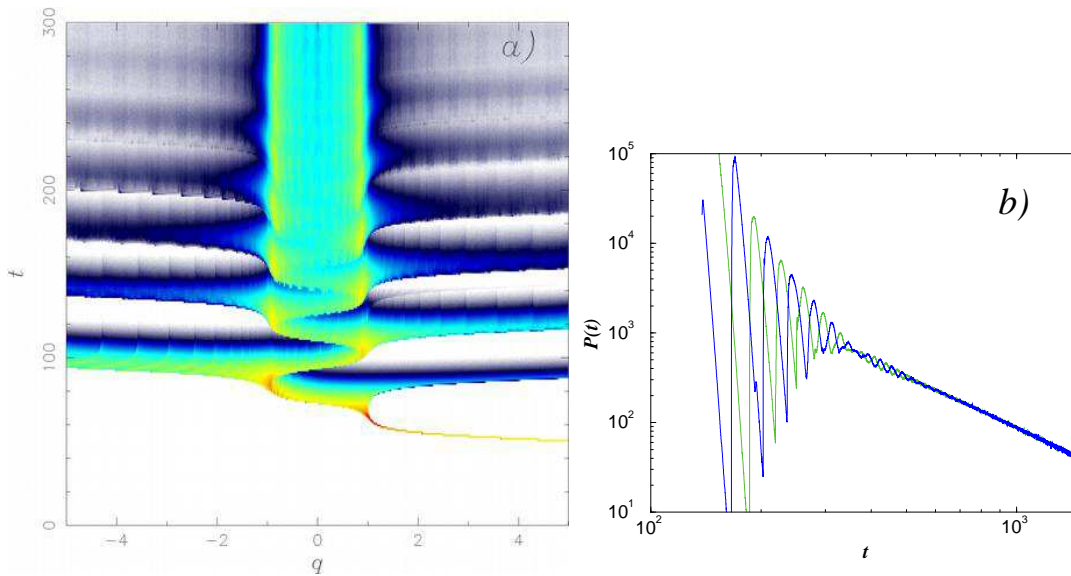


**Figure 10.** *a)* Classical density distribution in  $\rho_{cl}(q, t)$  for the model system eq. 8) in a logarithmic colour scale for  $A = 0.366$  corresponding to a development of  $-\log_3 \beta = 17$ . *b)* Outgoing flux of classical trajectories as a function of time  $P(t)$ , measured at  $q = -20$  (green) and  $q = 20$  (blue).

in Fig. 10-b in which we plot  $P(t)$  measured at  $q = \pm 20$ . The decay underlying the oscillations in  $P(t)$  is again of power-law nature, with a power of  $\approx 2$ .

Before testing our theoretical expectation for the period of the echoes we consider the quantum scattering process for this kicked system. For this purpose we use the unitary time evolution operator easily obtained for kicked systems. For one time step it can be written as three phases intertwined by Fourier transforms  $\mathcal{F}$ , which take us from coordinate to momentum space and back. Thus we obtain for the kernel of this operator in momentum-space

$$U(p', p) = \exp \left[ -\frac{i}{4\hbar} p'^2 \right] \mathcal{F} \exp \left[ \frac{i}{\hbar} AV(q) \right] \mathcal{F}^{-1} \exp \left[ -\frac{i}{4\hbar} p^2 \right]. \quad (11)$$

This expression is simple and very efficient if good fast Fourier transform (FFT) codes are used.

We shall analyze our scattering system in terms of wave packet dynamics, and use minimum uncertainty Gaussian wave packets given by

$$\Psi(q, 0) = \frac{1}{\pi^{1/4} \sigma^{1/2}} \exp \left[ -\frac{(q - q_0)^2}{2\sigma^2} + \frac{i}{\hbar} p_0 q \right]. \quad (12)$$

For a given value of the initial momentum  $p_0$ ,  $\sigma$  will determine the duration of the pulse. The value of  $\hbar$  will determine how near to the classical limit we operate. Recall that short pulses imply a poor energy resolution, while long ones can have fairly well defined energies. We can therefore use short pulses and consider the time evolution, or we can use long pulses and look at the energy dependence of some outgoing quantity. We shall start with the former.

In close analogy to the classical case we show in Fig. 11-*a* the quantum probability distribution in configuration space  $\rho_q(q, t)$  as a function of time in a logarithmic colour-scale code for  $A = 0.366$ ,  $\hbar = 0.01$ . The wave packet with  $\sigma = 2.5$  was initially placed at  $q_0 = 50$  with an incoming energy  $E_{\text{in}} = 0.40415$ . Again we clearly distinguish the incoming pulse, the part directly scattered at the barrier and another part that entered the well of the potential, but leaves directly to the left. At longer times we see an oscillating packet inside the well mimicking the behaviour of the classical density distribution but with an amplitude that corresponds to the classically forbidden region in phase space. Each time the wave packet returns to either one of the borders of the potential well (*i.e.*  $q = \pm 1$ ) an “echo” is emitted to infinity. This occurs alternately to the left and right of the potential well with a period that corresponds to half the orbital period. Since the quantum probability is rotating inside the stable island the information encoded in the period of the quantum scattering echoes will correspond to a winding number characteristic of the region of the island on which the probability is rotating. Therefore, we expect that due to quantum tunneling the period of the quantum echoes will be smaller than that of the classical case.

Again, in order to obtain a value for the period of the quantum scattering echoes, we measure the outgoing flux as a function of time  $P(t)$ , measured around  $q = \pm 20$ . This is shown in Fig. 11-*b*. The echoes emitted to left and right are in counter phase as expected. The decay of the quantum probability is exponential. This occurs at values of  $A$  for which the classical decay is power-law as expected for a mixed phase space situation and is an additional signature that tunneling has occurred. It is worthwhile mentioning that in our calculations we have not observed the  $1/t$  power law regime for intermediate times as found and discussed in [14].

We show quantum simulations with short pulses  $\sigma = 2.5$  for several values of the strength parameter  $A$ . In Fig. 12 we summarize our findings comparing the obtained values for the quantum echoes with the classical echoes and with the theoretical expectation of eq. 9. We display the obtained period of the classical (squares) and quantum (circles) echoes as a function of the development parameter of the ternary horseshoe  $\beta$  directly read off the horseshoe for the corresponding values of the parameter  $A$ . At low developments stages of the horseshoe the period of the quantum echoes is consistently shorter than for the classical echoes. As discussed, this shortening is to be expected as the quantum probability can tunnel through the classical invariant KAM surfaces and thus, test orbital periods inside the island. For the model in question the typical situation holds, in which this period decreases with the distance to the center of the island. This result is interesting by itself as the quantum scattering echoes could be used to scan the dynamics in the interior of the stable island which is by no means, accessible to classical experiments. We shall discuss this in more detail below. For cases in which the horseshoe is more developed the period of the quantum echoes turned to be longer than for the classical echoes. This may be a particular artifact of the structure of the chaotic layer of this model but, in any case here we approach to the region in which our theory ends to be valid. In Fig. 12 the straight line corresponds to the expected

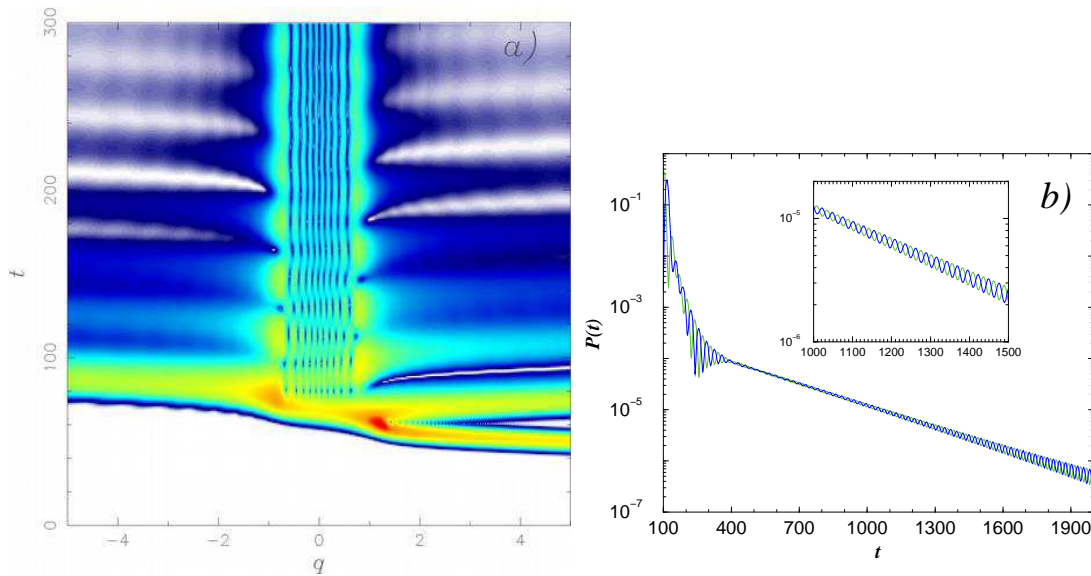


**Figure 11.** *a)* Quantum density distribution function in configuration space  $\rho_q(q, t)$  as a function of time for the model system of eq. 8 in a logarithmic colour scale for the same parameters as in Fig. 10. The incident wave-packet was initially set at  $q = 50$  and energy  $E_{in} = 0.40415$  corresponding to the energy domain of the incoming manifold of the classical horseshoe.  $\hbar = 0.01$  and  $\sigma = 2.5$ . *b)* Outgoing flux  $P(t)$  measured at  $q = -20$  (green) and  $q = 20$  (blue).

behaviour of eq. 9. The period of the classical echoes is found to be in good agreement within numerical accuracy.

So far, the incoming wave packets were chosen to be narrow in position space. This implies the good resolution obtained for observables as a function of time. However, we can also use long pulses that are narrow packets in momentum space, to obtain good energy resolution. In this case we have chosen as observable the quantum probability amplitude integrated over the potential well region at time  $t$  as a function of the asymptotic energy of the incident wave packet  $I_t(E_{in})$ . While this quantity shows a resonance spectrum very similar to the the  $S$ -matrix it turned out in our numerics, that we obtained better resolution with this quantity. In Fig. 13 we show  $I_t(E_{in})$  measured at  $t = 500$  with  $\sigma = 10$  for  $A = 0.366$  and  $\hbar = 0.01$ . The time at which  $I_t(E_{in})$  is measured is not relevant as long as the measure is performed after the direct scattering has subsided. If this is the case, the change in the position of the resonances is negligible as its amplitude decays very slowly. We find a group of narrow resonances periodically repeated in energy. The presence of these sharp resonances is an additional indication that tunneling between the regular and chaotic regions of the classical phase portrait occurs [15]. From  $I_t(E_{in})$  it is possible to extract two energy scales. The first and trivial scale corresponds to the width in energy of the group of resonances or to be more precise, to the energy length at which each resonance is repeated. This energy scale equals  $2\pi\hbar$  and correspond to the period of the kick that we have taken 1. In Fig. 13 the green horizontal bar measures this energy scale.

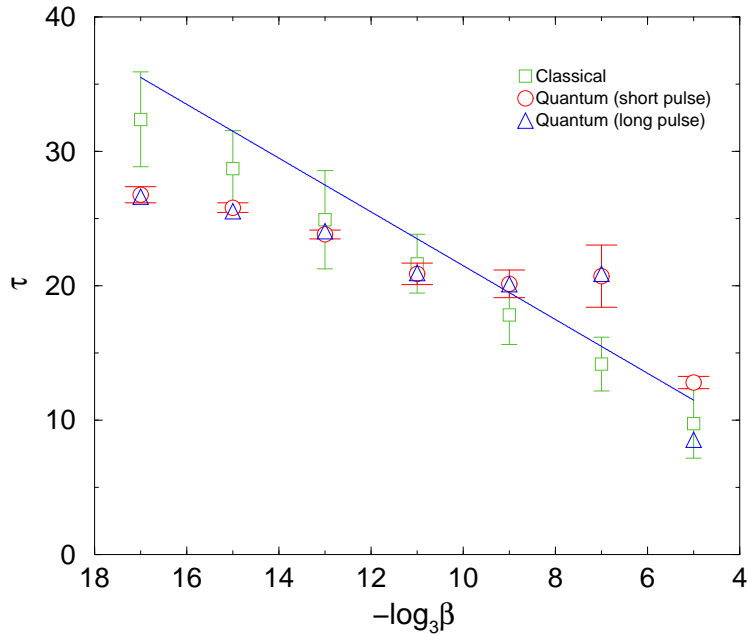


**Figure 12.** Period of the classical and quantum echoes  $\tau$ , for the model system of eq. 8. The squares correspond to the period of the classical echoes. The period of the quantum echoes was calculated from scattering simulations with short (circles) and long (triangles) pulses. The straight line corresponds to  $T$  given in eq. 9.

The second energy scale that can be extracted from  $I_t(E_{in})$  corresponds to the separation between resonances and, in analogy, it necessarily corresponds to  $2\pi\hbar/\tau$  with  $\tau$  the period of the quantum echoes. However, the energy separation between resonances decreases with energy. To understand this energy dependence we have carefully analyzed each resonance separately. In the inset of Fig. 13 an amplification of the first group of resonances is shown. Floquet formalism [19] applies to systems that, like our kicked model eq. 6, possess a time periodic potential. The translation invariance results in a description in all respects analogous to the Bloch formalism for spatially periodic systems. In the Floquet formalism these narrow resonances can be interpreted as the quasi-bound states associated to the system's potential. To analyse the structure the quasibound states have in phase space, we have calculated their Husimi distribution [20]. We prepare a long pulse with an incoming energy equal to the one of the resonance we want to study. At some time, after which the most of the probability has decayed we compute the Husimi distribution of the quantum probability inside the potential well. In Fig. 14 we show in a colour scale the obtained Husimi distribution for resonances 1, 4, 7 and 10 as labeled in the inset of Fig. 13. In Fig. 14 the Husimis are superimposed to the corresponding classical phase portrait in gray. From this figure a clear answer to the energy dependence emerges. Each resonance in the group corresponds to a quasibound state. On phase space they are ring-shape states around the center of the stable island. The quasibound state corresponding to the first resonance lives deep



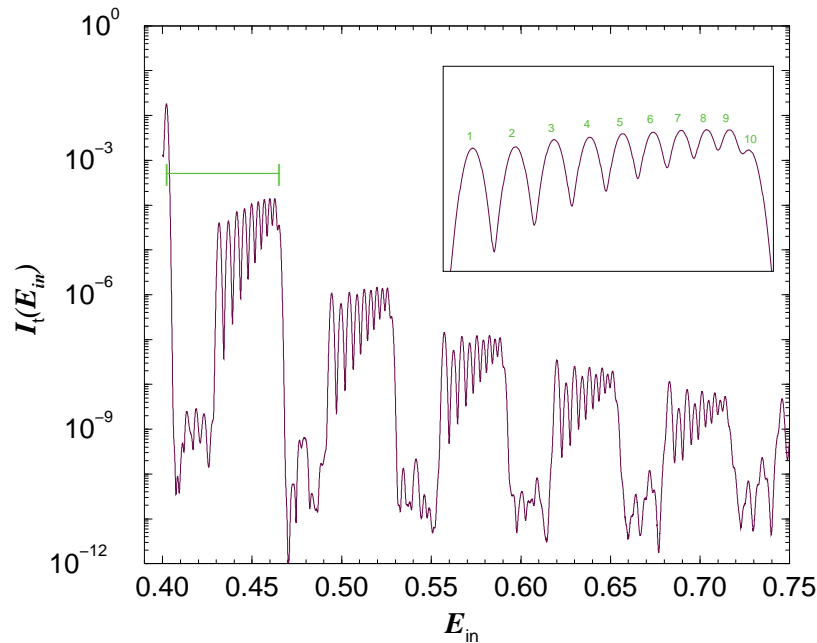


**Figure 13.** Quantum probability amplitude  $I_t$  inside the potential well as a function of the energy of the incident wave packet  $E_{in}$  measured at time  $t = 500$  for long pulse with  $\sigma = 10$ . The rest of the parameters are as in Fig. 11. The green bar correspond to a width of  $2\pi\hbar$  from the resonance that occur at the energy domain of the incoming manifold of the classical horseshoe. In the Inset an amplification of the first group of resonances have been labeled for discussion purposes.

inside the island while for the last resonance 10 the quasibound state covers the classical scattering layer. The more energetic the resonance is the further out the region on which it lives. Therefore, we can conclude that the energy scale associated to the period of the scattering echoes must correspond to the energy separation between those resonances associated to the most exterior quasibound states, *i.e.*, to the separation between the last two resonances in the group.

Following this strategy we have obtained  $I_t(E_{in})$  for the same values of the parameter  $A$  for which we have analysed the quantum scattering in terms of short pulses and measured the period of the echoes as  $\tau = 2\pi\hbar/\Delta E$  with  $\Delta E$  the separation between the last two resonances in the group. The results are shown in Fig. 12 as triangles. The correspondence between the results extracted from short and long pulses is excellent, thus opening the possibility to obtain the period of the quantum scattering echoes in the time or energy domain. It is worthwhile to mention that the first large resonance appearing in the spectrum of  $I_t(E_{in})$  has a classical interpretation. Indeed its energy corresponds to the asymptotic energy of the fringe in which the tendrils emerge along the outer branches of the invariant manifolds of the classical horseshoe. As indicated by the horizontal green bar in Fig. 13, the position of this “classical” resonance is a distance of  $2\pi\hbar$  from the last resonance, thus confirming the association of the period of the quantum echoes to the energy separation between the last resonances.



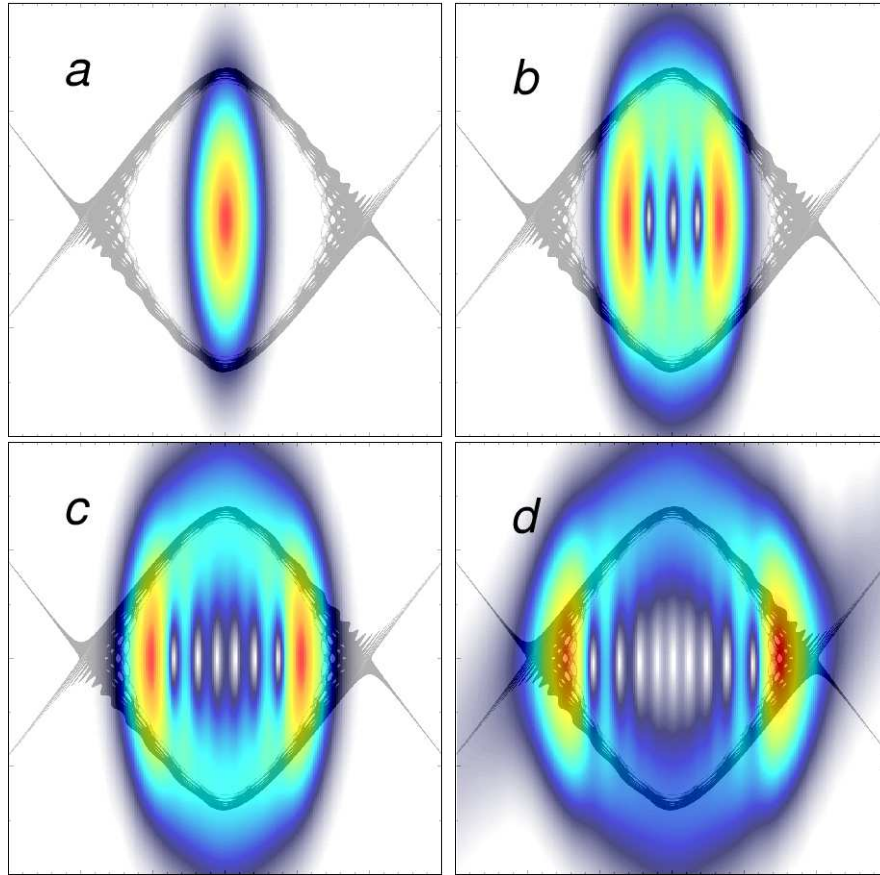


**Figure 14.** Husimi distribution for an incident long pulse with  $\sigma = 10.0$  superimposed to the classical phase portrait. The rest of the parameters are as in Fig. 11. The energy of the incident pulse was chosen as the energy of resonance: a) 1, b) 4, c) 7 and d) 10.

We want to call attention to the possibility to apply quantum scattering echoes as a tool to explore the dynamics in the interior of the island inaccessible to classical scattering trajectories. For the model system eq. 8 we have performed the following numerical experiment: As before, we target the potential well with a short pulse  $\sigma = 2.5$  with initial incoming momentum  $p_0$  and measure the outgoing quantum flux  $P(t)$  as a function of time. Applying a Fourier transformation to  $P(t)$  we obtain its frequency spectrum  $F(\nu)$ . As  $P(t)$  corresponds to the decay of the quantum probability that stays rotating around the stable island its Fourier spectrum simply tells us the frequency at which the quantum probability rotates. In Fig. 15 we show  $F(\nu)$  for five initial wave packets with different incoming momenta. What we observe is that the probability trapped in the potential well, rotates with a period which depends on the incoming momentum of the packet. Comparing the five spectra it is clear that the excited frequencies correspond to those of the quasibound states of the system. Indeed this is the case as it is confirmed in the inset of the same figure where the resonance spectrum of  $I_t(p_0)$  as a function of the incoming momentum is shown. Therefore, by measuring

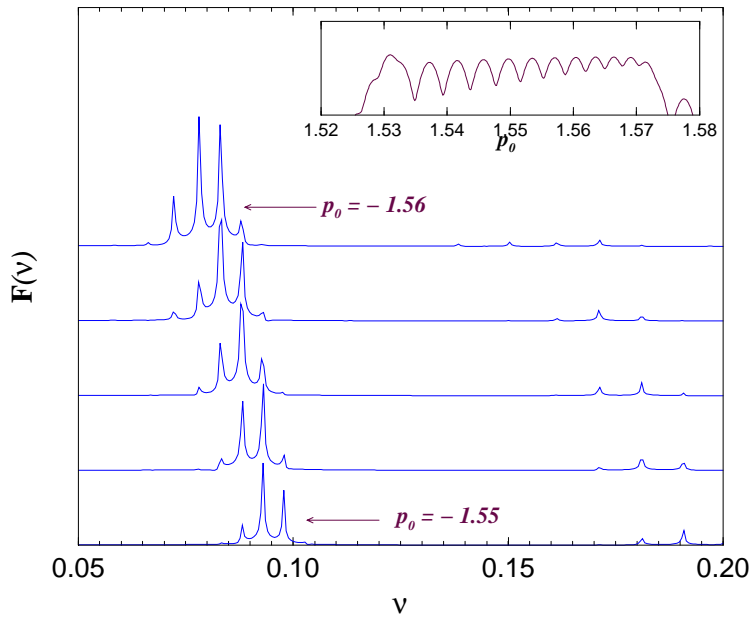


**Figure 15.** Fourier transform of the quantum outgoing flux  $P(t)$  for the model system of eq. 8 for  $A = 1.065$ . The spectra correspond to initial wave packets with different incoming momenta, from bottom to top:  $p_0 = -1.55$ ,  $p_0 = -1.5525$ ,  $p_0 = -1.555$ ,  $p_0 = -1.5575$  and  $p_0 = -1.56$ . The rest of the parameters are  $q_0 = 50$ ,  $\sigma = 2.5$  and  $\hbar = 0.01$ . In the inset we plot the first group of resonances appearing in  $I_t$ , calculated at  $t = 125$ . The first resonance at  $p_0 \sim 1.53$  corresponds to the classical resonance.

the period of the quantum echoes obtained from an incident packet that scans the incoming energy we can produce a map of the characteristic winding numbers in the interior of the island. In a sense, wave mechanics may be used as an "x-ray device" to study regions inaccessible in classical mechanics. Under certain circumstances this may be a way to solve the problem of finding the return time to the classical surface of section we encountered above, because the differential rotation time will converge to the period of the inner periodic orbit, which has the value  $2\Delta$  which we used successfully to approximate this time. Similar results could be obtained by Fourier transform of results in the energy domain, as touched upon in the conclusions.

As a final example we briefly comment the classical scattering in a billiard giving rise to a symmetric ternary horseshoe. A study of this particular example and its experimental realization will appear elsewhere [7]. The billiard in question consist of two boundaries: A Gaussian and a parabola given by

$$y(x) = \exp(-\alpha x^2) \tag{13}$$

$$y(x) = \gamma - \delta x^2 .$$

Both boundaries extend from  $-\infty$  to  $\infty$ . The shape of this billiard is shown inside Fig. 16 for some set of its parameters. This billiard has three fundamental periodic orbits, one in each neck and one in the center. The stability of the inner periodic orbit

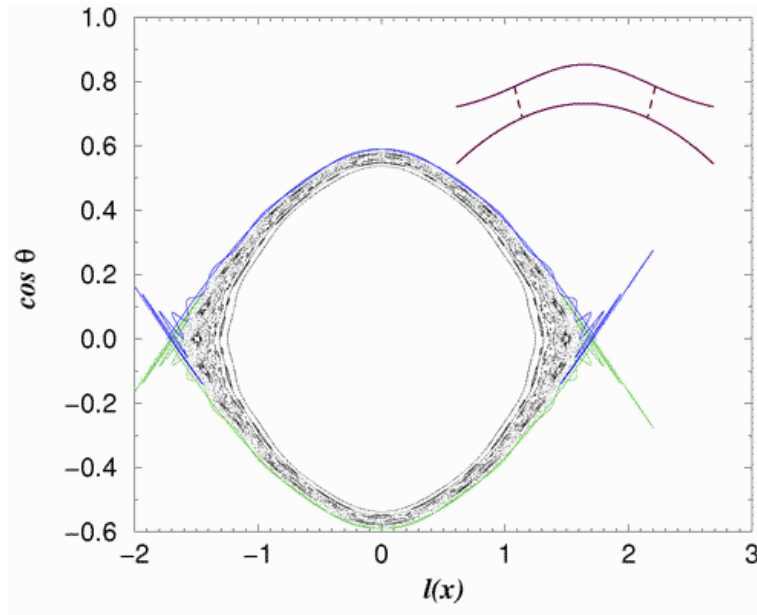


**Figure 16.** Classical horseshoe and phase portrait for the knee billiard for  $\alpha = 0.161$ ,  $\gamma = 0.2$  and  $\delta = 0.1$ . The development of the horseshoe is  $-\log_3 \beta = 8$ . The shape of the billiard is shown at the top right of the figure where the dashed lines correspond to the unstable periodic orbits.

corresponding to a vertical trajectory at  $x = 0$ , depends on the values for the local curvature of the boundaries. The other two periodic orbits, indicated in the figure as dashed lines are unstable for any set of the billiard's parameters and thus, give rise to a symmetric ternary horseshoe. In Fig. 16 we show this ternary horseshoe superimposed to the scattering layer given in Birkhoff coordinates over the lower (parabolic) boundary.

The phase portrait of this billiard shows a generic structure with an underlying ternary horseshoe. Therefore, the appearance of echoes is guaranteed. Again we have obtained the outgoing flux of classical trajectories as a function of time  $P(t)$ , measured at symmetric positions in the asymptotic region. This is shown in Fig. 17 in which the scattering echoes are evident. As before, the echoes emitted to the left are in counter phase with those emitted to the right.

## 5. Conclusions and outlook

In a soft chaos scattering situation, where a large central island exists, we find a self-pulsing effect, which we call scattering echoes. They can be measured experimentally, and can be used to make significant progress in the inverse scattering problem for such situations.

We understand the inverse scattering problem as the task to reconstruct information about the chaotic invariant set from asymptotic data. The approach presented is new in two aspects. First, it handles little developed horseshoes where a homoclinic tangle

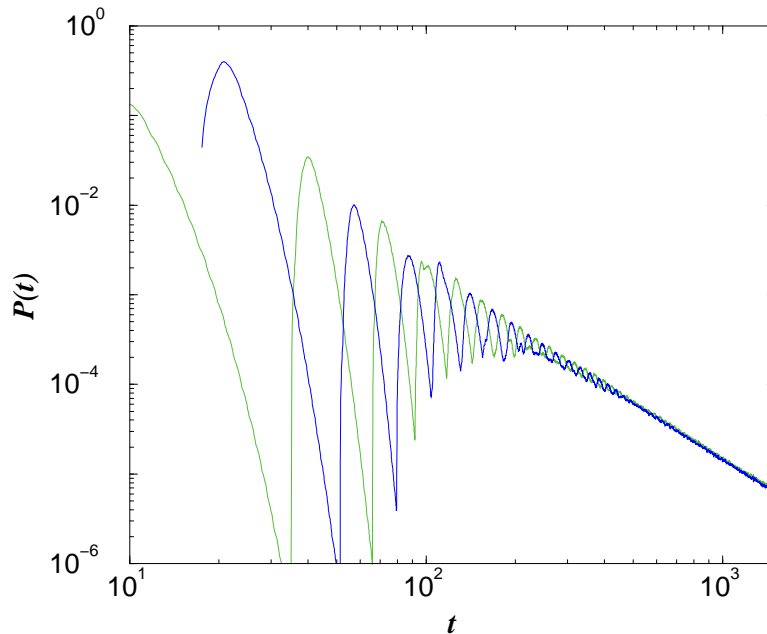


**Figure 17.** Outgoing flux of classical trajectories as a function of time for the knee billiard, measured at  $q = -20$  (blue) and  $q = 20$  (green).

encircles a large KAM island. Second, to our knowledge it is the first method for the inverse chaotic scattering problem which works for classical and quantum ( wave ) dynamics along the same idea.

We concentrate on systems described by binary and ternary symmetric horseshoes in a two dimensional Poincaré map. The generalization to asymmetric ternary horseshoes is simple and we have mentioned the essential equation for this case in eq. 10. More complicated generalizations would be necessary for billiards with more than two openings. Such systems can serve as models for rearrangement scattering where each opening represents one arrangement channel. The corresponding Poincaré map has a more complicated domain of several connected components which can lead to horseshoes of essentially complex structure. The treatment of the inverse problem for such systems remains an interesting open question. Another nontrivial generalization is the transition to systems with more than two important degrees of freedom. Yet the theory of chaotic scattering in higher dimensions is incipient [21].

The test of our ideas in laboratory experiments is in progress for the transmission of electromagnetic waves through open cavities [7]. Such experiments are typically done in the frequency domain, but if we use Fourier transforms to pass to the time domain, the following fascinating possibility exists: We measure a very long sequence of echoes. The first ones correspond to components of the wave, which only visit the outer regions of the homoclinic tangle. After longer time we measure components, which tunneled into the outer regions of the stable island. Signals leaving after ever longer times correspond to tunneling deep into the KAM island. Accordingly the change of

the distances between adjacent echoes during the measurement reflects the differential rotation of the various layers inside of the island. In this type of measurement the absorption which exists in any real experiment will set a limit to the maximal time (depth of penetration into the island) which can be reached. The problem of absorption might be circumvented by placing antennae into the interior of the interaction region. Of course, then the experiment is no longer a pure scattering experiment, and it would no longer be a testing ground for ideas for solving the inverse problem. However, it might be a worthwhile experiment for the analysis of tunneling of waves out of KAM islands. The only problem could be the distortion of the horseshoe dynamics by the presence of the antenna.

While microwave billiards present an obvious testing ground for our results, we expect, that scattering echoes of the type we discussed, will appear in other experiments in atomic and molecular physics, and that situations similar to the billiards can be set up in mesoscopics and for atoms in laser fields.

## Acknowledgments

We acknowledge useful discussions with F. Borondo, F. Leyvraz, P. Seba, A. Heine, T. Friedrich, A. Richter and H.-J. Stöckmann. Financial support by DGAPA-UNAM, project IN101603 and by CONACyT, project 25-192-E is acknowledged. C.M.-M. acknowledges a fellowship by DGEP-UNAM and the kind hospitality at the Centro Internacional de Ciencias (Cuernavaca) where part of this work was done.

- [1] C. Jung, C. Lipp and T.H. Seligman, *Ann. Phys.* **275** (1999) 151.
- [2] S. Smale, *Bull. Am. Math. Soc.* **73** (1967) 747.
- [3] C. Jung and H. Tapia, *Phys. Lett. A* **313** (2003) 198.
- [4] T. Bütikofer, C. Jung and T.H. Seligman, *Phys. Lett. A* **265** (2000) 76.
- [5] T. Tel, in *Directions in Chaos*, ed. H. Bai-Lin, Vol. 3, (World Scientific, 1990), p. 149.
- [6] C. Jung, C. Mejía-Monasterio and T.H. Seligman, *Europhys. Lett.* **55** (2001) 616.
- [7] C. Dembowski, B. Dietz, T. Friedrich, H.-D. Gräf, A. Heine, C. Mejía-Monasterio, M. Miski-Oglu, A. Richter and T. H. Seligman *to be published*.
- [8] B. Rüdiger and C. Jung, *J. Phys. A: Math. Gen.* **27** (1994) 55.
- [9] J. Moser *Stable and Random Motions in Dynamical Systems*, (Princeton U. Press) 1973.
- [10] A. J. Lichtenberg and M. A. Leiberman, *Regular and Chaotic Dynamics*, (Springer-Verlag 1991).
- [11] D.W. Noid, S.K. Gray and S. A. Rice, *J. Chem. Phys.* **84** (1986) 2642. S. K. Gray, S. A. Rice and D.W. Noid, *J. Phys. Chem.* **81** (1986) 1083. S. H. Tserigni, P. Gaspard and S. A. Rice, *J. Chem. Phys.* **92** (1990) 1775. I. Burghardt and P. Gaspard, *J. Chem. Phys.* **100** (1994) 6395. M. Dantus, R. M. Bowman, M. Gruebele and A. H. Zewail, *J. Chem. Phys.* **91** (1989) 437. S. A. Rice, P. Gaspard and K. Nakamura, *Adv. Class. Traj. Methods* **1** (1992) 215.
- [12] M.J. Davies, R.S. MacKay and A. Sannami, *Physica D* **52** (1991) 171.
- [13] G. Troll, *Chaos* **3** (1993) 459.
- [14] G. Casati, G. Maspero and D.L. Shepelyansky, *Phys. Rev. Lett.* **82** (1999) 524.
- [15] P. Seba, *Phys. Rev. E* **47** (1993) 3870.
- [16] B. Eckhardt *J. Phys. A* **20** (1987) 5971.
- [17] J.Rehacek, *Random & Comp. Dyn.*, **3** (1995) 35.
- [18] B. Chirikov and D.L. Shepelyansky, in *Proceedings of the IXth International Conference on*

*Nonlinear Oscillations, Kiev, 1981* [Naukova Dumka **2**, 420 (1984); C.F. Karney, *Physica D* **8** (1983) 360; B. Chirikov and D.L. Shepelyansky, *Physica D* **13** (1984) 395; R.S. MacKay, J.D. Meiss and I.C. Percival, *Physica D* **13** (1983) 55.

[19] G. Floquet, *Ann. l'Ecole Norm. Sup.*, **12** (1883) 47.

[20] K. Husimi, *Poc. Phys. Math. Soc. Jpn.* **22** ( 1940) 264.

[21] S. Wiggins, *Global Bifurcations and Chaos* (Springer-Verlag 1988).